

The role of soil amendments in limiting the leaching of agrochemicals: Laboratory assessment for copper sulphate and dicamba

*Original*

The role of soil amendments in limiting the leaching of agrochemicals: Laboratory assessment for copper sulphate and dicamba / Granetto, M., Bianco, C., Tosco, T.. - In: JOURNAL OF CLEANER PRODUCTION. - ISSN 0959-6526. - ELETTRONICO. - 474:(2024). [10.1016/j.jclepro.2024.143532]

*Availability:*

This version is available at: 11583/2994765 since: 2025-01-07T09:53:47Z

*Publisher:*

Elsevier Ltd

*Published*

DOI:10.1016/j.jclepro.2024.143532

*Terms of use:*

This article is made available under terms and conditions as specified in the corresponding bibliographic description in the repository

*Publisher copyright*

Elsevier postprint/Author's Accepted Manuscript

© 2024. This manuscript version is made available under the CC-BY-NC-ND 4.0 license  
<http://creativecommons.org/licenses/by-nc-nd/4.0/>. The final authenticated version is available online at:  
<http://dx.doi.org/10.1016/j.jclepro.2024.143532>

(Article begins on next page)

1 The role of soil amendments in limiting the leaching of  
2 agrochemicals: laboratory assessment for copper sulphate  
3 and dicamba

4 Monica Granetto, Carlo Bianco, Tiziana Tosco\*

5 *Department of Environmental, Land and Infrastructure Engineering (DIATI), Politecnico di Torino,*  
6 *Corso Duca degli Abruzzi, 24, 10129, Turin, Italy*

7 \* *Corresponding author: tiziana.tosco@polito.it*

8

9 Submitted to Journal of Cleaner Production

10

11 **Abstract**

12 Agriculture is among the major contributors to soil and groundwater pollution, primarily through the  
13 widespread leaching of pesticides and fertilizers from crops, as well as accidental releases from point sources.  
14 Therefore, alongside restrictions on the use of highly soluble agrochemicals and enhanced application  
15 guidelines, there is a significant demand for low-impact and cost-effective solutions aimed at reducing the  
16 mobility of agrochemicals in the soils. This study evaluates the potential of soil amendments—commonly  
17 used to enhance soil structural properties, water holding capacity, and fertility—to also absorb highly soluble  
18 pesticides, thereby controlling their leaching into the subsoil. Specifically, zeolite, biochar, and milled corncob  
19 were examined in laboratory tests under static (batch tests) and dynamic (column leaching tests) conditions  
20 to assess their effectiveness in adsorbing two widely used pesticides, copper sulphate and dicamba. Batch  
21 adsorption tests were performed using the amendments as pure materials and in mixtures with sand at  
22 various application rates (1 to 20% by weight). The highest affinity to copper sulphate was recorded for  
23 biochar, while dicamba exhibited a higher affinity to corncob, thanks to its higher content of organic carbon.  
24 Column leaching tests, performed at an amendment application rate of 5%, confirmed the different affinity  
25 observed in batch tests among pesticides and amended soil. Less than 2% of copper sulphate leached out  
26 from biochar- and zeolite-sand columns, while a recovery of 10% and 56% was observed for the corncob-  
27 sand mixture and for pure sand, respectively. Dicamba leaching from biochar- and corncob-sand columns  
28 was halved compared to pure sand. In conclusion, the tested soil amendments resulted highly effective in  
29 reducing pesticide leaching, opening the way for their possible applications in agriculture to reduce or  
30 prevent both diffuse and punctual contamination.

31

32 **Keywords**

33 Soil amendments; Zeolite; Biochar; Corncob; Pesticide leaching; Pesticide sorption

34 **Highlights**

35 Biochar and corncob show high affinity to dicamba and limit its leaching in lab tests

36 Zeolite-amended sand highly retain Cu sulphate and retention is partly irreversible

37 Unprocessed agricultural waste can effectively control leaching of organic pesticides

38

## 39 Introduction

40 Preserving the high quality of surface water and groundwater represents a current global challenge.  
41 Agriculture, along with urban and industrial activities, is among the major pollution sources (Sethi and Di  
42 Molfetta, 2019), including both diffuse emissions associated with excessive load of nutrients (in particular  
43 phosphorus and nitrogen), pesticides and pharmaceuticals (Dordio and Carvalho, 2013), and accidental spills  
44 at well-localized contamination roots (e.g. storage vessels or sprayer tanks, parking or loading areas, etc.)  
45 (Ritter, 1988). Several technologies are currently available to manage point source releases and treat  
46 collected streams of contaminated water, similar to those applied to industrial or civil effluents. Conversely,  
47 controlling contaminant spread from diffuse sources is an intrinsically challenging target. To this aim, soil  
48 amendments, in particular processed or raw agricultural waste (e.g. sawdust, mowing, biochar, etc.) and  
49 minerals (e.g. zeolites) show good potential (Ahmad et al., 2014; Sud et al., 2008). Their effectiveness in  
50 adsorbing and/or immobilizing organic and inorganic contaminants is already exploited in industrial  
51 wastewater treatments and remediation of contaminated soils and sediments (Cao et al., 2011; Ghosh et al.,  
52 2011). Conversely, in the agricultural sector, their primary use is currently as soil quality improvers, to  
53 increase soil water retention capacity and control fertilizer release to plants (Diacono and Montemurro,  
54 2010). Surprisingly, little attention has been devoted so far to their potential interactions with pesticides, and  
55 more in general to limit contaminant release from agricultural sources (Kookana et al., 2011). Among the  
56 limited literature available on this topic, notable findings include the biochar capacity to increase glyphosate  
57 adsorption (with a partition coefficient 33% higher in biochar-amended soil than in untreated soil) (Kumari  
58 et al., 2016) and the ability of Ca-hydroxide, Ca-bentonite, and natural zeolites to significantly increase the  
59 copper immobilization compared to control soil (Lahori et al., 2017). Moreover, the leaching potential of  
60 fipronil, a broad spectrum insecticide, was reduced by 97% in in coarse sand amended with cereal straw,  
61 compared to the unamended soil (Joshi et al., 2016). In this framework, this study intends to advance  
62 knowledge on the role of soil amendments in controlling leaching of soluble agrochemicals.

63 Among adsorbents derived from agricultural waste, biochar, produced through pyrolysis of plant residues, is  
64 the most known and used soil amendment. Its porous structure and surface properties render it an effective,

65 low cost material for removal of both organic (Tong et al., 2019) and inorganic compounds (Liu et al., 2022).  
66 Similar advantages could be obtained also with mineral amendments like zeolites, whose exploitation in  
67 agriculture increased in the last two decades (Mondal et al., 2021). Zeolites, sometimes after surface  
68 modification, are often used in industrial wastewater treatments in deep bed filtration, and as soil  
69 amendments for nutrients adsorption and controlled release (Ferretti et al., 2020; Wang and Wang, 2022).  
70 However, only a few studies investigated their adsorption capacity toward agricultural contaminants such as  
71 pesticides (Cataldo et al., 2021).

72 Despite the good performance of biochar and zeolites as adsorbents, their production processes (either  
73 biochar pyrolysis or zeolite mining), milling and surface functionalization require non negligible energy input.  
74 Consequently, in the name of a higher sustainability, perspective soil amendments produced from  
75 agricultural waste with minimal energy demand would be highly desired. Milled corncob, with its large  
76 availability and highly porous structure, is a promising option. It is currently exploited mainly for its high  
77 energy content and as a source for biochar production, but to the authors' knowledge no previous study is  
78 available on the efficacy of unprocessed corncob as an adsorbent. For this reason, it has been selected along  
79 with biochar and zeolite to be investigated in this study.

80 Copper sulphate and dicamba, both characterized by high solubility and thus leaching potential, were studied  
81 in this work as representative of, respectively, inorganic and organic pesticides. Copper, broadly used as  
82 fungicide in organic agriculture, is among the priority pollutants categorized by USEPA. Copper leaching is  
83 influenced by the precipitation intensity and duration, the chemistry of infiltrating water (ionic strength, pH),  
84 and the presence and dynamics of dissolved organic matter (DOM), which has a high affinity with copper  
85 (Aldrich et al., 2002). High infiltration was reported in sandy soils, with 47.9% of copper leaching from  
86 columns spiked with 600 mg kg<sup>-1</sup> of Cu (Bakshi et al., 2014). Dicamba, an herbicide targeting broadleaf weeds  
87 in crops like maize and sorghum, is highly soluble in water, with consequent high leaching potential (Granetto  
88 et al., 2022). Its use in conjunction with 2,4-D has increased in USA since 2002 in response to the notable rise  
89 in the number of herbicide-resistant weed biotypes (Hoy et al., 2015). Moreover, the introduction of

90 dicamba-resistant crops, such as soybeans and cotton, in Brazil (CTNBio, 2023) and other parts of the world,  
91 suggests an overall increase in the application of this herbicide in the next years (Aguiar et al., 2023).

92 This research presents laboratory studies on the potentiality of soil amendments in limiting the leaching of  
93 soluble pesticides in static (batch tests) and dynamic conditions (column leaching tests), elucidating the  
94 dependence of adsorption mechanisms and removal efficiency on morphology, composition and physical-  
95 chemical properties and application ratio of the amendments. Despite the laboratory scale of the study, a  
96 few preliminary conclusions were drawn in view of a full-scale application of the studied amendments for  
97 pesticide immobilization.

98

99

## 100 **Materials and methods**

### 101 ***Materials***

102 Three natural amendments were supplied by local producers, including biochar (Ronda Engineering; nominal  
103 size < 5mm; source: pyrolysis at 700 °C of untreated woodworking waste), zeolite (Zeocel Italia; nominal size:  
104 0.6-2mm; nominal composition: 70±5% chabazite, 2±1 % phillipsite, 5±2% sanidine, 3±1% augite, 2±1% illite),  
105 and corncob (Agrindustria; nominal size: 50% 180-610µm and 50% 610-850µm; source: fibrous part of the  
106 corn ear after extraction, drying and milling).

107 Silica sand (Dorsilit 8, Dorfner, Germany;  $d_{10}$ ,  $d_{50}$  and  $d_{90}$  equal respectively to 0.415, 0.45 and 0.5 mm) was  
108 used to mimic the soil structure, as pure material or mixed with the amendments. The cleaning procedure is  
109 detailed in Beryani et al (2022). The following chemicals were used: copper sulphate pentahydrate  
110  $\text{CuSO}_4 \cdot 5\text{H}_2\text{O}$  (Scharlab, Spain, purity > 99.5%), dicamba (Alfa Chemistry, US, purity > 99.5%), citric acid (Chem  
111 Lab, Belgium, purity > 99.5%), trisodium citrate dehydrate (Supelco, ACS grade), Zincon (Alfa Aesar), HCl  
112 (Merck EMSURE, ACS grade) and NaOH (Honeywell Fluka, ACS grade).

113

114 ***Characterization of the amendments and amendment-sand mixtures***

115 Zeolite and biochar samples were hand-crushed in a ceramic mortar prior use and sieved to discard the  
116 fraction larger than 2mm. Corncob was not further milled since already provided in adequate size by the  
117 producer. Particle size distribution (PSD) was measured via dry sieving for all samples. Particle shape and  
118 elemental chemical composition were investigated using SEM-EDS microscopy (JEOL, Japan). To this aim, air-  
119 dried samples were deposited on a stub using carbon (zeolite) or aluminium (biochar and corncob) tape, to  
120 avoid interferences of the tape composition with EDS elemental peaks. Powder X-Ray diffraction (Rigaku  
121 SmartLab SE) was performed on grounded samples using a CuK $\alpha$  radiation source ( $\lambda = 1.54 \text{ \AA}$ ) operating at  
122 40 kV and 30 Ma with scan range 5°-90° and scan step of 0.01°. Particle density was determined applying a  
123 modified liquid pycnometer (BLAUBRAND, type Gay-Lussac, volume of 50cm<sup>3</sup>, calibrated according to DIN  
124 ISO3507) method proposed by Heiskanen (Heiskanen, 1992).

125 The three amendments were then added separately to the sand at different application rates (1–2–5–10–  
126 20% mass fraction) and hand-mixed up to complete homogenization. Bulk density, water holding capacity,  
127 pH and salt content of pure amendments, pure sand and of the mixtures were determined according to the  
128 European Biochar Certificate (EBC) guidelines for sustainable biochar production (Schmidt, 2015). Further  
129 details are provided in paragraph 1 in Supporting Information.

130

131 ***Batch adsorption tests***

132 Adsorption tests were performed in 50 ml sealed glass vials, prepared by adding 2.5 g of solid material (pure  
133 sand, pure amendment or a mixture of the two) to 25 ml of pesticide solution ranging 124 to 624 mg/l for  
134 copper sulphate and 250 to 1500 mg/l for dicamba, corresponding to the application ranges commonly used  
135 in agriculture for the two compounds. For each pesticide, six different initial concentrations were tested in  
136 the respective range. The vials were continuously mixed with an overhead shaker (Rotax 6.8, Velp Scientifica,  
137 Italy) at 15 rpm for 24 hours to ensure equilibrium between liquid and solid phases. The contact time was

138 selected based on kinetic adsorption tests, performed using the same experimental procedure at the  
139 maximum concentration of the two pesticides in contact with the pure amendments (results reported in  
140 paragraph 2 in Supporting Information). After 24 h, the samples were centrifuged at 6000 rpm for 20 mins  
141 (Neya 16 centrifuge, REMI, India) and filtered with a PTFE syringe filter with 0.45  $\mu\text{m}$  mesh to remove  
142 suspended colloids. The supernatants were then analysed for residual copper or dicamba concentrations: a  
143 colorimetric method, described in paragraph 3 in Supporting Information, was adapted from Ghasemi et al.  
144 (2003) for copper, while dicamba was directly measured with Uv-VIS spectrophotometer (Specord S600,  
145 Analytic Jena, Germany) at 280.5 nm (Figure S3-3). Given the concentration in liquid phase and the liquid  
146 volume, the concentration in solid phase was calculated through mass balance.

147 The experimental results were modelled with Freundlich and Langmuir isotherms. The Freundlich model,  
148 suitable for adsorption on heterogeneous surfaces (Vadivelan and Kumar, 2005), was expressed as

$$149 \quad s_{eq} = K_f C_e^{1/n} \quad (\text{eq. 1})$$

150 where  $s_{eq}$  is the adsorbed concentration [-] in equilibrium with the liquid concentration  $C_e$  [ $\text{ML}^{-3}$ ],  $K_f$  is the  
151 adsorption capacity [ $\text{M}^{-1/n} \text{L}^{3/n}$ ] and  $1/n$  is the Freundlich constant [-], being  $1/n < 0.1$  for strongly favourable  
152 adsorption,  $0.1 < 1/n < 0.5$  for favourable adsorption,  $1/n > 0.5$  for unfavourable adsorption.

153 The Langmuir model, suitable to describe monolayer adsorption (Liu, 2006), was expressed as

$$154 \quad s_{eq} = \frac{q_{max} L C_e}{1 + L C_e} \quad (\text{eq. 2})$$

155 where  $q_{max}$  is the maximum adsorption capacity [-] and  $L$  the Langmuir adsorption coefficient [ $\text{L}^3 \text{M}^{-1}$ ].

156 In order to shade further light on adsorption mechanisms, the zeta potential of biochar, zeolite and corncob  
157 diluted to 1 g/l in 3 mM NaCl solution was measured at varying pH (modified by dropwise addition of 50 mM  
158 HCl or NaOH) using Dynamic Light Scattering (Malvern, Zetasizer NANO ZSP).

159

160

161 ***Column leaching tests***

162 Copper and dicamba leaching tests were performed in glass columns (inner diameter 4.1 cm) packed  
163 with 320 g of dry sand or of a sand-amendment mixture at 5% application rate. For the mixtures, 16 g of  
164 water were added prior packing to allow a slight cohesion between sand and amendment, thus avoiding  
165 layering of the two materials during column filling. Column preparation included the following steps: (i) the  
166 wet mixture was introduced in small amounts (~20 g) and compacted with a pestle layer by layer; (ii) upward  
167 flow (0.2 ml/min) was established until complete saturation; (iii) the column length (~18 cm) was measured,  
168 and the column weighted for saturated water content determination. The columns were then left draining  
169 by gravity until field capacity was reached. Unsaturated downward flow (0.4 ml/min, corresponding to an  
170 infiltration rate of 0.028 cm/min) was then established. A tracer test was performed injecting KBr at constant  
171 concentration and the breakthrough electrical conductivity curve was recorded. The unsaturated water  
172 content, unsaturated pore volume (PV) time, saturated hydraulic conductivity, and dispersivity were  
173 determined via least-squares fitting of the breakthrough curve (BTC) to the classical advection-dispersion  
174 equation in unsaturated porous media (paragraph 4 in SI) using Hydrus 1D (Simunek et al., 2013).

175 After the tracer test, a copper sulphate or dicamba solution (depending on the test) was injected for at least  
176 7.5 h at constant concentration of 624 mg/l or 1500 mg/l, respectively, followed by a flushing with deionized  
177 water for 7.5 h. The column outflow was collected using a fraction collector and samples analysed for copper  
178 and dicamba with the same methods used for adsorption tests.

179 At the end of the tests, the columns were extruded and dissected to determine copper and dicamba profiles.  
180 Copper was extracted from the solid by using a modified version of the sequential extraction method  
181 proposed by Silveira (Silveira et al., 2006), including the following steps: (i) addition of 0.1 M CaCl<sub>2</sub> and mixing  
182 for 24h to promote ion exchange, (ii) addition of 1M NaOAc (Carlo Erba, purity > 99%) and mixing for 5h for  
183 the extraction of Cu(II) adsorbed on grain surface, and (iii) addition of NaOCl (Carlo Erba, solution at 30%) at  
184 90°C for 2h to promote release from the organic matter. Cu precipitated in oxide/hydroxide form is expected  
185 not to be recovered. Dicamba was extracted in one step using acetonitrile:CaCl<sub>2</sub> 10 mM 70:30 w/w with  
186 continuous mixing for 24h. All suspensions were centrifuged at 6000 rpm for 20 min before the analysis.

187 Copper and dicamba BTCs were modelled with Hydrus 1D (Simunek et al., 2012) using a two-site  
 188 adsorption equilibrium model, having one site characterized by instantaneous adsorption (eq. 4) and the  
 189 other one by kinetic adsorption (eq. 5 and 6):

$$190 \quad \frac{\partial \theta c}{\partial t} + \rho \frac{\partial s^e}{\partial t} + \rho \frac{\partial s^k}{\partial t} = \frac{\partial}{\partial z} \left( \theta D \rho \frac{\partial c}{\partial z} \right) - \frac{\partial q c}{\partial z} - \varphi \quad (\text{eq. 3})$$

$$191 \quad s^e = f_e F(c) \quad (\text{eq. 4})$$

$$192 \quad \rho \frac{\partial s^k}{\partial t} = \alpha_k \rho (s_e^k - s^k) - \varphi_k \quad (\text{eq. 5})$$

$$193 \quad s_e^k = (1 - f_e) K_d c \quad (\text{eq. 6})$$

194 where  $s^e$  is the solute concentration adsorbed on the instantaneous (equilibrium) adsorption site expressed  
 195 as mass of adsorbed solute per unit mass of solid [-],  $F(c)$  is the corresponding adsorption isotherm (linear,  
 196 Langmuir, etc.),  $f_e$  is the fraction of exchangeable sites in equilibrium with the liquid phase [-],  $s^k$  is the  
 197 concentration adsorbed on the kinetic (non-equilibrium) adsorption site [-] and  $s_e^k$  is the corresponding  
 198 adsorbed concentration at equilibrium for the kinetic adsorption site [-] expressed by the linear isotherm of  
 199 eq. 6,  $\alpha_k$  is the first order rate constant of the kinetic site [ $T^{-1}$ ],  $K_d$  is the partition coefficient for the kinetic  
 200 site [ $L^3 M^{-1}$ ],  $\varphi$  and  $\varphi_k$  are the sink/source terms accounting for generic reactions [ $ML^{-3} T^{-1}$ ]. The total adsorbed  
 201 concentration is  $s = s^e + s^k$ .

202

## 203 **Results and discussion**

### 204 ***Characterization of the amendments and amendment-sand mixtures***

205 The milled biochar showed a highly heterogeneous morphology (Figure 1a), with larger particles exhibiting a  
 206 highly intra-porous structure, and smaller ones characterized by an elongated, flat shape. The PSD analysis  
 207 indicated  $d_{10}$ ,  $d_{50}$  and  $d_{90}$  equal to 0.15, 0.7 and 1.9 mm respectively (Figure S5-1). The XRD pattern (Figure  
 208 1b) showed the typical biochar composition, including mainly aromatic hydrocarbons and graphite-like  
 209 carbon structures (Gao et al., 2020). The humped trend in the region  $15^\circ < \theta/2\theta < 30^\circ$  is due to the amorphous

210 carbonaceous structure resulting from pinewood pyrolysis. The high peak at 26.5° can be associated with  
211 pyrolysis of inorganic impurities, mainly graphite (Mohan et al., 2018), while additional peaks at 29°, 36°, 39°,  
212 44° and 48° can be associated with superficial Ca-based compounds such as CaCO<sub>3</sub> and CaO (Tran et al., 2015;  
213 Waqas et al., 2021).

214 Hand-milled zeolite showed a distinctly cubic shape, with well-defined angles and smoothed faces due to  
215 mechanical crushing (Figure 1c), and particle size lower than 1 mm ( $d_{10}$ ,  $d_{50}$  and  $d_{90}$  respectively equal to 0.07,  
216 0.4 and 0.9 mm, Figure S5-2). The XRD pattern (Figure 1d) was consistent with that of Ca-chabazite type  
217 zeolite, characterized by a stronger diffraction response at  $\theta/2\theta < 15^\circ$  compared to K-chabazite, as reported  
218 by previous crystallographic studies (Leyva-Ramos et al., 2008). This is confirmed by EDS results (Figure S5-  
219 4), reporting the presence of Ca (3.2% on average). Peaks in the XRD spectrum other than those characteristic  
220 of chabazite were identified at  $\theta/2\theta = 23.3^\circ - 30.4^\circ$ . A good agreement was found with sanidine at 23.3°,  
221 27.5°, 27.9° and 29.7°, with illite at 29.9° and 34.14° and with augite at 27.5°, 39.7°, 30.4° and 35.5°,  
222 coherently with the nominal sample composition and with previous studies (Ramos et al., 2015).

223 Corncob (not further milled) showed a higher heterogeneity and irregularity in terms of both PSD ( $d_{10}$ ,  $d_{50}$   
224 and  $d_{90}$  equal to 0.2, 0.55 and 0.85 mm, Figure S5-3) and morphology compared to biochar and zeolite. The  
225 SEM analysis (Figure 1e) identified the presence of elongated particles interspersed with more compact,  
226 jagged ones. The first ones could be attributed to the central pitch part of corncob, the latter to the external  
227 glume and wood ring. The XRD pattern (Figure 1f) denoted a highly amorphous lignocellulose material (in  
228 particular alfacellulose) identified by two peaks at  $\theta/2\theta = 16^\circ$  and  $22^\circ$  (Menezes et al., 2017). Crystalline  
229 peaks at 36° and 44° could be traced back to Ca-containing impurities on corncob surface.

230 Figure 2 reports the results of the sand-amendment mixture characterization (bulk density, water holding  
231 capacity, electrical conductivity and pH) obtained following the EBC guidelines for sustainable biochar  
232 production. The grain density, measured with a liquid pycnometer, resulted in the following trend: sand (2.6  
233 g/cm<sup>3</sup>) > zeolite (2.35 g/cm<sup>3</sup>) > biochar (1.6 g/cm<sup>3</sup>) > corncob (1.52 g/cm<sup>3</sup>). The amendment addition to the  
234 sand significantly affected the bulk density of columns dry-packed with the mixtures (Figure 2a), which

235 decreased linearly from 1.53 g/cm<sup>3</sup> for pure sand with increasing amendment application ratio, reaching  
236 1.33, 1.07 and 0.81 g/cm<sup>3</sup> for 20% application rates of zeolite, corncob and biochar, respectively. The highest  
237 bulk density reduction (45.3%) was obtained with biochar, even though the lowest grain density was  
238 measured for corncob, suggesting that the bulk density of the mixtures was not a mere weighted mean of  
239 the densities of sand and amendment but, rather, was significantly affected by the amendment particle  
240 shape. The theoretical porosity corresponding to the measured bulk density (Figure S5-5) increased from  
241 0.41 for pure sand to 0.48, 0.52 and 0.66 for zeolite, corncob and biochar, respectively, at 20% application  
242 rate, thus confirming the beneficial effect of amendments (and in particular of biochar and corncob) in terms  
243 of reduced bulk density and increased porosity, and consequently reduced soil compaction, higher aeration  
244 and potentially lower risk for soil erosion.

245 The water holding capacity (WHC) increased with increasing the amendment application rates (Figure 2b),  
246 and the general observed WHC trend was corncob>biochar>zeolite. At the highest application rates (20%),  
247 WHC of 0.34, 0.54 and 0.55 g/g were measured respectively for zeolite-, corncob- and biochar-sand mixtures,  
248 corresponding to a WHC increase of 72%, 172% and 177% compared to pure sand. For biochar, both intra-  
249 porosity, inter-porosity and the highly irregular surface morphology are expected to have positively affected  
250 the biochar-sand mixture WHC (Liu et al., 2017; Verheijen et al., 2019). Similar considerations could be drawn  
251 for corncob-sand mixtures, even though no previous literature is available on the characterization of  
252 unprocessed corncob as soil amendment. Conversely, the (limited) effect of zeolite on the WHC of the  
253 mixtures is mainly attributable to a decrease in particle size, and consequently increase in capillary water  
254 retention (Ibrahim and Alghamdi, 2021).

255 The water electrical conductivity of the pure amendments in contact with water was equal to 29, 165 and  
256 1015  $\mu$ S/cm for zeolite, biochar and corncob, respectively. The conductivity of the amendment-sand mixtures  
257 increased significantly with increasing the amendment application rates, except for zeolite-containing  
258 samples, which did not show any significant trend (Figure 2c). Conversely, the high conductivity of pure  
259 biochar and corncob denoted a high propensity to free and exchange ions in solution. It is worth to mention  
260 that higher values of conductivity, and so salt content, could lead both to a higher potential for ions exchange

261 and ionic species adsorption, but also to a reduced germinability and damage to crop due to induced salt  
262 stress (Buss et al., 2016).

263 The pH value of the pure materials in contact with water was 7.5, 8.4, 6.7 and 4.7 for sand, biochar, zeolite  
264 and corncob, respectively. Coherently, the mixtures showed slightly alkaline pH for biochar, nearly neutral  
265 for zeolite and acidic for corncob (Figure 2d). The biochar-sand mixture pH was close to pure biochar pH at  
266 all application rates, suggesting that biochar is able to buffer sand, contrary to corncob and zeolite, which  
267 showed decreasing pH with increasing application rates.

268

## 269 ***Adsorption tests***

### 270 ***Copper sulphate***

271 The copper sulphate adsorption isotherms for the mixtures are reported in Figure 3a-c as adsorbed  
272 concentration  $s_{eq}$  (i.e. adsorbed  $CuSO_4$  mass over the total mass of adsorbent, i.e. sand + amendment) against  
273  $CuSO_4$  residual concentration in liquid phase at equilibrium. Adsorption on pure sand was minimal compared  
274 to the mixtures. The adsorption capacity followed the trend biochar>zeolite>corncob. Biochar isotherms  
275 showed a trend toward saturation (Figure 3a) for application rates lower than 5%. For rates higher than 10%  
276 the same trend can be hypothesized, even though the plateau was not reached since the tests were  
277 performed exploring the environmentally-relevant range of  $CuSO_4$  concentrations. A similar saturative trend  
278 was shown by zeolite-sand mixtures (Figure 3b) but not by corncob-amended sand (Figure 3c).

279 The experimental isotherms were least-squares fitted to the Langmuir and Freundlich models. The model  
280 parameters are reported in Supporting Information in Table S6-1 and their trends as a function of the  
281 amendment application rates are reported in Figure 4. As a general rule, both models resulted in very high  
282  $R^2$  values for most isotherms, with a few exceptions. A slightly better fitting with the Langmuir model  
283 compared to Freundlich (see  $R^2$  values) suggests a monolayer adsorption mechanism on a homogeneous  
284 adsorbent surface, coherently with other studies on  $CuSO_4$  interaction with various adsorbents (Wang et al.,  
285 2012; Zand and Abyaneh, 2020).

286 Biochar showed a general better fitting with the Langmuir model compared to the Freundlich one,  
 287 particularly for rates < 20%. Adsorption was unfavourable ( $1/n \geq 0.5$ ) for biochar rates  $\geq 20\%$ , and favourable  
 288 ( $1/n < 0.5$ ) for rates < 10% (Figure 4a). Conversely, the Freundlich adsorption coefficient  $K_f$  showed a bimodal  
 289 trend in the range 0.09 to 0.74 g l<sup>1/n</sup> with a peak at application rate of 5% (Figure 4b). Increasing  $q_{max}$  with  
 290 increasing application rate was also observed (Figure 4c). Zeolite showed a very good fitting for both  
 291 Freundlich and Langmuir isotherms for application rates from 1% to 20%, with slightly higher R<sup>2</sup> values for  
 292 the Freundlich model at medium-to-high application rates, and particularly for rates > 5%. The fitted values of  
 293  $1/n$  increased with increasing application rates in the range 0.15-0.3, thus suggesting that copper adsorption  
 294 on zeolite is a favourable process (Figure 4a). As for corncob, the Langmuir model showed a general better  
 295 fitting compared to the Freundlich one, with saturation concentration  $q_{max}$  significantly lower than those  
 296 obtained for biochar (Figure 4c).

297 To further investigate the adsorption capacity and mechanisms, the isotherms were reported also in terms  
 298 of adsorbed CuSO<sub>4</sub> normalized to the mass of amendment (i.e. excluding sand),  $s_{eq,norm}$ , calculated as

299 
$$s_{eq,norm} = \frac{s_{eq} - s_{eq,AR=0\%}(1 - AR)}{AR}$$

300 where  $s_{eq,AR=0\%}$  is the adsorbed concentration measured in the absence of amendment (i.e. when sand is the  
 301 only solid in the batch). An unexpected trend of the results was obtained (Figures 3d-f): with decreasing  
 302 application rates,  $s_{eq,norm}$  increased for all tested materials. This suggests that adsorption is more efficient  
 303 in the presence of a low adsorbent content in the solid fraction, even though the adsorption on sand grains  
 304 is minimal.

305 In general, the main expected mechanisms of CuSO<sub>4</sub> removal from water include surface adsorption (due to  
 306 electrostatic attraction and ion exchange), and precipitation of Cu oxides and hydroxides at favourable  
 307 hydrochemical conditions (Tan et al., 2015; Zhao et al., 2020). For both mechanisms, pH plays a key role. The  
 308 pH was acidic in all our tests due to the presence of CuSO<sub>4</sub> in solution, and was slightly affected by the  
 309 amendment application rates (Figure S6-1): in particular, pH was close to 5 for pure sand and increased with  
 310 increasing both zeolite and biochar application rate toward plateau values of approximately 6 and 7,

311 respectively, but decreased toward approximately 4.5 for corncob-sand mixtures (coherently with the more  
312 acidic pH of corncob). Concerning copper precipitation, Jiang et al. (Jiang et al., 2016) indicate that, for acidic  
313  $\text{CuSO}_4$  solutions in contact with biochar, the formation of insoluble  $\text{Cu}(\text{OH})_2$  is expected starting from pH  
314 above 6. Thus, the pH values of our tests would explain the limited Cu removal observed for pure sand and  
315 corncob (Figure 3f), and the higher one for zeolite and biochar (Figures 3d and 3e), even though the pH values  
316 measured for zeolite- and biochar-sand mixtures are not high enough to suggest a predominance of  
317 precipitation as removal mechanism. The pH influences the surface charge of the adsorbent and thus the  
318 surface adsorption due to electrostatic attraction toward dissolved copper ions. Zeta potential, which can be  
319 used as an indirect measurement of surface charge, was negative for all amendments in our tests (Figure S5-  
320 6), and decreased with increasing pH, suggesting a higher affinity of the amendments to the copper cations  
321 at higher pH. Again this trend would explain the corncob isotherms but not those obtained for zeolite and  
322 biochar. Consequently, other properties controlling surface adsorption are likely to play the major role in our  
323 tests. Among them, the specific surface area of the amendment is likely the parameter controlling adsorption  
324 capacity. It was observed that during the adsorption experiments the particle size of the amendment was  
325 reduced: optical microscope analysis of corncob particles before and after the adsorption tests evidenced a  
326 clear decrease in size (Figure S6-2 in Supporting Information); particle size distributions obtained via image  
327 processing (ImageJ, National Institutes of Health, US) showed that the difference is more pronounced at low  
328 application rate (5%) and negligible at the highest application rate (20%) (Figure S6-3). This can be explained  
329 by sand acting as ball milling, thus reducing amendment particle size during mixing with the overhead shaker  
330 (Shan et al., 2016): the higher the sand content in the sample, the more effective the milling. Higher copper  
331 loading potential at decreasing particle size was also reported previously for biochar, and was attributed to  
332 a larger surface area available and easier accessibility to pores for finer adsorbents (Zou et al., 2006).

333

#### 334 ***Dicamba***

335 The dicamba adsorption isotherms (Figure 5) show a higher overall adsorption capacity for corncob  
336 and biochar, followed by zeolite. For all tested materials, the removal efficiency increased with increasing

337 application rate, similarly to what observed for CuSO<sub>4</sub>. The contribution of sand to dicamba adsorption is  
338 minor, even though not negligible, compared to the three amendments (see black dotted isotherms in Figure  
339 5). For biochar- and corncob-sand mixtures (Figures 5a and 5c), the isotherms showed an asymptotic trend  
340 toward a saturation concentration for rates <10% and <5%, respectively. The saturative trend is further  
341 evidenced when the isotherms are normalized to the mass of amendment (Figure 5d and f). Conversely,  
342 zeolite isotherms were distinctly linear at all tested application rates, without any evident saturative  
343 behaviour (Figures 5b and e). It is worth observing that the removal efficiency of pure zeolite is lower than  
344 the other two pure amendments, but for low application rates (up to 2%) the removal efficiency of zeolite-  
345 sand mixtures (Figure 5b) was comparable to or higher than the others. This is reflected by remarkably higher  
346 normalized isotherms for zeolite at low application rates (Figure 5e).

347         The overall increasing adsorption efficiency of the adsorbents with decreasing application rates, as  
348 evidenced in Figures 5d-f, is in line with the results obtained for CuSO<sub>4</sub>, and confirms the key role of sand-  
349 mediated milling of the amendments in increasing the sorption efficiency in batch tests. However, the effect  
350 of comminution alone is not sufficient to explain all the results reported in Figures 5d-f, and in particular the  
351 overall reduced adsorption efficiency of biochar compared to corncob and zeolite. A key role in this sense is  
352 likely played by pH: dicamba in solution exhibits an acidic behaviour (Azejjel et al., 2008), with pKa equal to  
353 1.98 (Carrizosa et al., 2001). The dissociated dicamba molecule assumes a negative charge, that contrasts  
354 with the negative surface charge of zeolite/biochar/corncob. Thus, the dicamba adsorption is favoured when  
355 the compound is present in its molecular form, rather than when dissociated, and consequently at strongly  
356 acidic pH. Figure S6-4 in Supporting Information reports the trends for the pH measured in batch tests as a  
357 function of amendment application rates. For pure sand, the sample pH was 2.8, close to pKa. For all  
358 amendments, the pH increased with increasing application rate. As for biochar, pH rapidly approached  
359 neutrality for application rates higher than 5%, corresponding to a predominantly dissociated form of  
360 dicamba and thus to a lower affinity of the molecule to the amendment. Correspondingly, biochar exhibited  
361 the lowest normalized isotherms among the three tested materials (Figure 5d). For zeolite and corncob, the  
362 pH remained close to 3 for application rates lower than 5%. Correspondingly, the normalized isotherms of

363 Figures 5e and f showed higher adsorbed concentrations at low application rates compared to biochar. This  
364 finding suggests that, along with the optimal adsorbent milling obtained at low application rates, also pH  
365 played a fundamental role in controlling dicamba adsorption potential.

366 The modelling of dicamba isotherms with Langmuir and Freundlich equations (coefficients in Table  
367 S6-2 in Supporting Information, trends with application rates in Figure 6) showed a good fitting for both  
368 models and for all the three materials, with slightly higher  $R^2$  values for the Langmuir model. For all zeolite-  
369 sand mixtures, linear adsorption was confirmed, being always  $1/n > 1$  (Figure 6a). The Freundlich adsorption  
370 coefficient  $K_f$  slightly decreased for biochar- and corncob-sand mixtures, and increased for zeolite-sand  
371 mixtures, with increasing application rate (Figure 6b). Corncob and biochar showed  $1/n < 1$ , increasing toward  
372 the unit with increasing application rates, thus suggesting adsorption of pseudo-linear type.

373

#### 374 ***Leaching tests***

##### 375 ***Column hydrodynamic characterization***

376 The hydrodynamic parameters of the columns in leaching tests in unsaturated conditions are reported in  
377 Table 1. A higher water content  $\theta$  for the biochar-sand column compared to others was expected according  
378 to the higher amendment WHC, higher biochar porosity and heterogeneous particle structure. The saturated  
379 hydraulic conductivity  $K_s$  was higher for pure sand and decreased progressively for corncob-, zeolite-, and  
380 biochar-sand mixtures, in accordance with previous literature (Sarabi and Sepaskhah, 2012; Yan et al., 2021).  
381 Conversely, the hydrodynamic dispersivity  $\alpha$  was similar in all tests.

382

##### 383 ***Copper sulphate leaching tests***

384 Figure 7a reports the breakthrough curves of copper sulphate in the four columns as a function of the injected  
385 unsaturated pore volumes (PVs). In general, the ability of the amendment-sand mixture to retain  $\text{CuSO}_4$   
386 followed the order sand < corncob-sand < zeolite-sand / biochar-sand mixtures. In pure sand, a relevant delay

387 in the breakthrough of CuSO<sub>4</sub> was observed, with  $C/C_0 > 0$  after 1.5 PVs, suggesting the occurrence of  
388 reversible equilibrium adsorption. A fairly constant concentration  $C/C_0 \sim 0.9$  was then measured for the entire  
389 duration of the injection step, indicating the occurrence, in parallel, of reversible equilibrium adsorption and  
390 kinetic irreversible adsorption or of precipitation. For zeolite and biochar, an almost null breakthrough was  
391 observed, with no CuSO<sub>4</sub> release even during post-flushing with deionized water, thus suggesting that CuSO<sub>4</sub>  
392 was irreversibly adsorbed and/or precipitated in the tested hydrochemical conditions. Negligible  
393 breakthrough was observed also for the sand-corncob column for 4.5 PVs, followed by a limited  
394 breakthrough. However, during flushing a significant desorption occurred, indicating in this case a weaker  
395 and partly reversible interaction between Cu and corn cob.

396 Relevant additional information can be obtained from the profiles of retained concentration of CuSO<sub>4</sub>,  
397 obtained dissecting the columns at the end of the leaching tests (Figure 7b). An almost constant copper  
398 concentration was detected along the vertical direction in pure sand ( $\sim 0.09$  mg/g) and for the corn cob-sand  
399 mixture ( $\sim 0.29$  mg/g, except for the deepest 4 cm). It is worth noticing that in both tests a non-negligible  
400 copper breakthrough concentration was measured at the end of injection, thus suggesting the two columns  
401 reached saturation along the entire column (for sand) or at least in its upper part (for the corn cob-sand  
402 mixture). Conversely, a different profile shape was observed for zeolite- and biochar-sand mixtures: in both  
403 cases, a higher Cu concentration was retained in the first 6 cm and negligible concentrations in the deepest  
404 part of the column, thus suggesting that biochar and zeolite have a much higher sorption capacity and column  
405 saturation was not reached during the test.

406 A closer analysis of the percentage of Cu recovered in each step of the sequential extraction method (aimed  
407 at recovering Cu aliquots retained due to different phenomena) provides additional information on the  
408 retention mechanisms (Figure S7-1 in Supporting Information). In all tests, the highest recovery was obtained  
409 in the first extraction step, aimed at promoting Cu(II) release via ion exchange. This predominance is  
410 particularly evident for corn cob and biochar, confirming the higher ion exchange capacity of these  
411 amendments compared to pure sand and zeolite. For the second extraction, aimed at releasing Cu adsorbed  
412 on mineral surfaces, the highest recovery was obtained for pure sand, followed by zeolite-, biochar- and

413 corncob-sand mixtures, indicating a slightly higher affinity of Cu to sand compared to zeolite surface. In the  
414 third extraction, aimed at extracting Cu adsorbed on the organic matter, the largest recovery percentage, as  
415 expected, was obtained for corncob. In all tests, and particularly for zeolite- and biochar-sand mixtures, a  
416 non-negligible fraction of Cu (Table 1) was not recovered at column outflow nor in the extraction procedure,  
417 suggesting that Cu precipitation in the form of oxides/hydroxides (which cannot be extracted by none of the  
418 methods adopted in the three steps) also partly occurred.

419 The breakthrough curve for pure sand was modelled using eq. 3 - 6 with one instantaneous (equilibrium)  
420 adsorption site (eq. 4) following a Langmuir isotherm, and one kinetic adsorption site (eq. 5). The fitting was  
421 satisfactory (Figure S7-2) with  $R^2 = 0.91$ . For the equilibrium site, the Langmuir parameters obtained were  
422  $q_{\max} = 4.02 \cdot 10^{-1} \text{ mg/g}$  and  $L = 1.66 \cdot 10^{-3} \text{ l/mg}$ , similar to the values obtained in batch tests for  $\text{CuSO}_4$  adsorption  
423 onto pure sand (Table S6-1). As for the kinetic site,  $\alpha_k = 1.29 \cdot 10^{-3} \text{ min}^{-1}$  and  $\varphi_k = 2.37 \cdot 10^{-3} \text{ min}^{-1}$  were  
424 obtained. The fraction of instantaneous adsorption sites where adsorption  $f_e$  was equal to 0.42, in agreement  
425 with the similar percentages of Cu recovery obtained in the first and second steps of the sequential extraction  
426 method.

427

#### 428 ***Dicamba***

429 Contrary to  $\text{CuSO}_4$  leaching tests, dicamba showed a significant breakthrough in all tested columns,  
430 corresponding to an overall lower affinity to the tested amendments (Figure 8a). No evident retardation was  
431 observed for pure sand and zeolite-sand mixture, while breakthrough was retarded for biochar- and  
432 corncorb-sand mixtures, with a retardation factor equal to 1.8 and 2.5, respectively. Beside retardation,  
433 which suggests the occurrence of instantaneous equilibrium adsorption, all breakthrough curves also showed  
434 a steady-state concentration plateau lower than the injected one, suggesting the concomitant occurrence of  
435 kinetic adsorption. From a qualitative point of view, the affinity of dicamba for the sorbent materials  
436 confirmed the same trend corncob>biochar>zeolite evidenced by batch tests, and by mass balances (Table  
437 1).

438 Figure 8b reports the vertical profile of retained dicamba at the end of the leaching tests. The profile for the  
439 corncob-sand mixture was not determined due to interference with other substances released by the  
440 corncob matrix. As a general trend, higher adsorption was observed in the upper part of the columns, where  
441 higher concentrations in pore water were present, even though concentrations are not negligible also at  
442 higher depths. The non-negligible concentrations of adsorbed dicamba measured along the column at the  
443 end of the test confirm the presence of two concurrent adsorption mechanisms (instantaneous and kinetic,  
444 the second being partly irreversible) hypothesized based on breakthrough curves: if adsorption was totally  
445 reversible, no significant retained concentration should have been measured, having breakthrough curves  
446 reached negligible values at the end of all tests.

447 The breakthrough curves of all dicamba leaching tests were modelled assuming the same mechanisms used  
448 for  $\text{CuSO}_4$  (parameter in Table S7-1, modelled curves in Figure S7-3 in Supporting Information). The fitting  
449 was visually satisfactory with  $R^2 > 0.95$  for all tests except for the sand-corn-cob mixture. The first-order rate  
450 constant for dissolved phase  $\alpha_k$  was higher for sand and sand-zeolite mixtures compared to biochar- and  
451 corncob-sand columns, suggesting that the latter materials reach faster equilibrium for the kinetic site  
452 compared to biochar- and corncob-sand columns. Comparing batch and column equilibrium adsorption  
453 parameters, and in particular the maximum adsorption capacity  $s_{\text{max}}$  (Figure 9a), it can be observed that in all  
454 cases the  $q_{\text{max}}$  values obtained in batch were higher than those obtained in columns, but with the same trend,  
455 likely due to the better and longer contact between adsorbents and dicamba solutions.

456

## 457 **Conclusions**

458 In this study, zeolite, biochar and corncob were used to adsorb and reduce the mobility in water and soil of  
459 two pesticides, namely copper sulphate and dicamba. These amendments were mixed with silica sand at  
460 different application rates. A general decrease in bulk density and a notable increase in water holding  
461 capacity were observed with increasing application rates, particularly for biochar and corncob. This suggests  
462 their higher potential for enhancing water storage in fields during drought conditions. Conversely, zeolite

463 showed minimal impact on both bulk density and water holding capacity. The addition of amendments also  
464 significantly altered the pH. Thus, the physical and chemical effects of adding amendments to sand or soil in  
465 crop fields must be taken carefully into account, particularly in the presence of plants and crops with specific  
466 tolerance thresholds to salt/pH/soil humidity.

467 The ability of the different mixtures to adsorb pesticides were first tested in batch. The amendment initial  
468 particle size distribution, application rate and the way of mixing used during adsorption test played crucial  
469 roles in the adsorption tests. In particular, head-over-head mixing allowed a significant reduction of  
470 amendment particle size due to friction with sand, thus enhancing adsorption rates, particularly at the lowest  
471 application rates. This finding evidences the importance of a careful evaluation of the results of batch  
472 adsorption tests, particularly when extrapolating their results to larger scales (column or field), due to the  
473 high impact of the specific operating conditions on the results. Highly charged amendments, such as biochar  
474 and zeolite, showed a higher affinity with copper, while dicamba was highly adsorbed by corncob due to its  
475 high organic matter content. The Langmuir adsorption model best fitted the experimental results for both  
476 copper sulphate and dicamba, suggesting a monolayer adsorption onto amendment surfaces.

477 Preliminary column leaching tests were conducted to assess the amendments' effects under hydrodynamic  
478 conditions. The results confirmed the higher affinity of biochar and zeolite for copper sulphate, with  
479 negligible leaching of copper from the column, compared to sand and sand-corn cob columns. For dicamba,  
480 higher retardation factor and consequently higher retention were observed in the corncob-sand mixture. In  
481 field conditions, this would result in longer retention of dicamba in the top soil, thus making its  
482 biodegradation more favourable.

483 In conclusion, natural soil amendments can be used not only to improve the physical-chemical characteristics  
484 of the soil, as currently practiced in some agronomic techniques, but also to enhance adsorption of pesticides  
485 in the soil, thus limiting the spreading of both diffuse and local contaminations in agricultural settings. The  
486 results of this study also highlight the potential benefits of combining multiple amendments at the field scale,

487 where diverse types of pesticides are applied, to limit the overall leaching of agrochemicals into deeper soil  
488 and groundwater.

#### 489 Cited literature

- 490 Aguiar, A.C.M. de, Silva, E.M.G. da, Barcellos Júnior, L.H., Paula, D.F. de, Souza, P.S.R. de, Guimarães, T.,  
491 Ovejero, R.F.L., Palhano, M.G., Silva, A.A. da, Mendes, K.F., 2023. Sorption, leaching, and  
492 degradation of dicamba in two Brazilian soils: A study into soil layers. *Crop Protection* 174, 106393.  
493 <https://doi.org/10.1016/j.cropro.2023.106393>
- 494 Ahmad, M., Rajapaksha, A.U., Lim, J.E., Zhang, M., Bolan, N., Mohan, D., Vithanage, M., Lee, S.S., Ok, Y.S.,  
495 2014. Biochar as a sorbent for contaminant management in soil and water: A review. *Chemosphere*  
496 99, 19–33. <https://doi.org/10.1016/j.chemosphere.2013.10.071>
- 497 Aldrich, A.P., Kistler, D., Sigg, L., 2002. Speciation of Cu and Zn in Drainage Water from Agricultural Soils.  
498 *Environmental Science & Technology* 36, 4824–4830. <https://doi.org/10.1021/es025813x>
- 499 Azejjel, H., Aatouf, N., Draoui, K., Rodriguez-Cruz, S., Sánchez-Martín, M., 2008. Influence of soil properties  
500 on the adsorption of two ionisable herbicides by Moroccan soils. *Fresenius Environmental Bulletin*  
501 17, 1627–1633.
- 502 Bakshi, S., He, Z.L., Harris, W.G., 2014. Biochar Amendment Affects Leaching Potential of Copper and  
503 Nutrient Release Behavior in Contaminated Sandy Soils. *Journal of Environmental Quality* 43, 1894–  
504 1902. <https://doi.org/10.2134/jeq2014.05.0213>
- 505 Beryani, A., Bianco, C., Casasso, A., Sethi, R., Tosco, T., 2022. Exploring the potential of graphene oxide  
506 nanosheets for porous media decontamination from cationic dyes. *Journal of Hazardous Materials*  
507 424, 127468. <https://doi.org/10.1016/j.jhazmat.2021.127468>
- 508 Buss, W., Graham, M.C., Shepherd, J.G., Mašek, O., 2016. Suitability of marginal biomass-derived biochars  
509 for soil amendment. *Science of The Total Environment* 547, 314–322.  
510 <https://doi.org/10.1016/j.scitotenv.2015.11.148>
- 511 Cao, X., Ma, L., Liang, Y., Gao, B., Harris, W., 2011. Simultaneous immobilization of lead and atrazine in  
512 contaminated soils using dairy-manure biochar. *Environ Sci Technol* 45, 4884–4889.  
513 <https://doi.org/10.1021/es103752u>
- 514 Carrizosa, M.J., Koskinen, W.C., Hermosin, M.C., Cornejo, J., 2001. Dicamba adsorption–desorption on  
515 organoclays. *Applied Clay Science* 18, 223–231. [https://doi.org/10.1016/S0169-1317\(01\)00037-0](https://doi.org/10.1016/S0169-1317(01)00037-0)
- 516 Cataldo, E., Salvi, L., Paoli, F., Fucile, M., Masciandaro, G., Manzi, D., Masini, C.M., Mattii, G.B., 2021.  
517 Application of Zeolites in Agriculture and Other Potential Uses: A Review. *Agronomy* 11, 1547.
- 518 Diacono, M., Montemurro, F., 2010. Long-term effects of organic amendments on soil fertility. A review.  
519 *Agronomy for Sustainable Development* 30, 401–422. <https://doi.org/10.1051/agro/2009040>
- 520 Dordio, A., Carvalho, A.J., 2013. Constructed wetlands with light expanded clay aggregates for agricultural  
521 wastewater treatment. *The Science of the total environment* 463–464, 454–61.  
522 <https://doi.org/10.1016/j.scitotenv.2013.06.052>
- 523 Ferretti, G., Keiblinger, K.M., Faccini, B., Di Giuseppe, D., Mentler, A., Zechmeister-Boltenstern, S., Coltorti,  
524 M., 2020. Effects of Different Chabazite Zeolite Amendments to Sorption of Nitrification Inhibitor  
525 3,4-Dimethylpyrazole Phosphate (DMPP) in Soil. *Journal of Soil Science and Plant Nutrition* 20, 973–  
526 978. <https://doi.org/10.1007/s42729-020-00184-3>
- 527 Gao, Y., Xiao, Y., Mao, K., Qin, X., Zhang, Yuan, Li, D., Zhang, Yanhui, Li, J., Wan, H., He, S., 2020.  
528 Thermoresponsive polymer-encapsulated hollow mesoporous silica nanoparticles and their  
529 application in insecticide delivery. *Chemical Engineering Journal* 383, 123169.  
530 <https://doi.org/10.1016/j.cej.2019.123169>
- 531 Ghasemi, J., Ahmadi, S., Torkestani, K., 2003. Simultaneous determination of copper, nickel, cobalt and zinc  
532 using zincon as a metallochromic indicator with partial least squares. *Analytica Chimica Acta* 487,  
533 181–188. [https://doi.org/10.1016/S0003-2670\(03\)00556-7](https://doi.org/10.1016/S0003-2670(03)00556-7)

- 534 Ghosh, U., Luthy, R.G., Cornelissen, G., Werner, D., Menzie, C.A., 2011. In-situ Sorbent Amendments: A New  
535 Direction in Contaminated Sediment Management. *Environ. Sci. Technol.* 45, 1163–1168.  
536 <https://doi.org/10.1021/es102694h>
- 537 Granetto, M., Serpella, L., Fogliatto, S., Re, L., Bianco, C., Vidotto, F., Tosco, T., 2022. Natural clay and  
538 biopolymer-based nanopesticides to control the environmental spread of a soluble herbicide.  
539 *Science of The Total Environment* 806, 151199. <https://doi.org/10.1016/j.scitotenv.2021.151199>
- 540 Heiskanen, J., 1992. Comparison of three methods for determining the particle density of soil with liquid  
541 pycnometers. *Communications in Soil Science and Plant Analysis* 23, 841–846.  
542 <https://doi.org/10.1080/00103629209368633>
- 543 Hoy, J., Swanson, N., Seneff, S., 2015. The High Cost of Pesticides: Human and Animal Diseases. *Poultry,  
544 Fisheries & Wildlife Sciences* 03. <https://doi.org/10.4172/2375-446X.1000132>
- 545 Ibrahim, H.M., Alghamdi, A.G., 2021. Effect of the Particle Size of Clinoptilolite Zeolite on Water Content  
546 and Soil Water Storage in a Loamy Sand Soil. *Water* 13. <https://doi.org/10.3390/w13050607>
- 547 Jiang, S., Huang, L., Nguyen, T.A.H., Ok, Y.S., Rudolph, V., Yang, H., Zhang, D., 2016. Copper and zinc  
548 adsorption by softwood and hardwood biochars under elevated sulphate-induced salinity and  
549 acidic pH conditions. *Chemosphere* 142, 64–71.  
550 <https://doi.org/10.1016/j.chemosphere.2015.06.079>
- 551 Joshi, V., Srivastava, A., Srivastava, P.C., 2016. Potential of some soil amendments in reducing leaching of  
552 fipronil to groundwater. *International Journal of Environmental Science and Technology* 13, 631–  
553 638. <https://doi.org/10.1007/s13762-015-0883-1>
- 554 Kookana, R.S., Sarmah, A.K., Van Zwieten, L., Krull, E., Singh, B., 2011. Chapter three - Biochar Application to  
555 Soil: Agronomic and Environmental Benefits and Unintended Consequences, in: Sparks, D.L. (Ed.),  
556 *Advances in Agronomy*. Academic Press, pp. 103–143. <https://doi.org/10.1016/B978-0-12-385538-1.00003-2>
- 558 Kumari, K.G.I.D., Moldrup, P., Paradelo, M., Elsgaard, L., de Jonge, L.W., 2016. Soil Properties Control  
559 Glyphosate Sorption in Soils Amended with Birch Wood Biochar. *Water, Air, & Soil Pollution* 227,  
560 174. <https://doi.org/10.1007/s11270-016-2867-2>
- 561 Lahori, A.H., Zhang, Z., Guo, Z., Li, R., Mahar, A., Awasthi, M.K., Wang, P., Shen, F., Kumbhar, F., Sial, T.A.,  
562 Zhao, J., Guo, D., 2017. Beneficial effects of tobacco biochar combined with mineral additives on  
563 (im)mobilization and (bio)availability of Pb, Cd, Cu and Zn from Pb/Zn smelter contaminated soils.  
564 *Ecotoxicology and Environmental Safety* 145, 528–538.  
565 <https://doi.org/10.1016/j.ecoenv.2017.07.071>
- 566 Leyva-Ramos, R., Jacobo-Azuara, A., Diaz-Flores, P.E., Guerrero-Coronado, R.M., Mendoza-Barron, J.,  
567 Berber-Mendoza, M.S., 2008. Adsorption of chromium(VI) from an aqueous solution on a  
568 surfactant-modified zeolite. *Colloids and Surfaces A: Physicochemical and Engineering Aspects* 330,  
569 35–41. <https://doi.org/10.1016/j.colsurfa.2008.07.025>
- 570 Liu, G.C., Pan, M.Q., Song, J.Y., Guo, M.Y., Xu, L.N., Xin, Y.J., 2022. Investigating the effects of biochar  
571 colloids and nanoparticles on cucumber early seedlings. *Sci Total Environ* 804.  
572 <https://doi.org/10.1016/j.scitotenv.2021.150233>
- 573 Liu, Y., 2006. Some consideration on the Langmuir isotherm equation. *Colloids and Surfaces A:  
574 Physicochemical and Engineering Aspects* 274, 34–36.  
575 <https://doi.org/10.1016/j.colsurfa.2005.08.029>
- 576 Liu, Z., Dugan, B., Masiello, C.A., Gonnermann, H.M., 2017. Biochar particle size, shape, and porosity act  
577 together to influence soil water properties. *PLOS ONE* 12, e0179079.  
578 <https://doi.org/10.1371/journal.pone.0179079>
- 579 Menezes, D.B., Brazil, O.A.V., Romanholo-Ferreira, L.F., de Lourdes T. M. Polizeli, M., Ruzene, D.S., Silva,  
580 D.P., Costa, L.P., Hernández-Macedo, M.L., 2017. Prospecting fungal ligninases using corncob  
581 lignocellulosic fractions. *Cellulose* 24, 4355–4365. <https://doi.org/10.1007/s10570-017-1427-2>
- 582 Mohan, D., Abhishek, K., Sarswat, A., Patel, M., Singh, P., Pittman, C.U., 2018. Biochar production and  
583 applications in soil fertility and carbon sequestration – a sustainable solution to crop-residue  
584 burning in India. *RSC Adv.* 8, 508–520. <https://doi.org/10.1039/C7RA10353K>

585 Mondal, M., Biswas, B., Garai, S., Sarkar, S., Banerjee, H., Brahmachari, K., Bandyopadhyay, P.K., Maitra, S.,  
586 Brestic, M., Skalicky, M., Ondrisik, P., Hossain, A., 2021. Zeolites Enhance Soil Health, Crop  
587 Productivity and Environmental Safety. *Agronomy* 11. <https://doi.org/10.3390/agronomy11030448>  
588 Ramos, C.G., Querol, X., Oliveira, M.L.S., Pires, K., Kautzmann, R.M., Oliveira, L.F.S., 2015. A preliminary  
589 evaluation of volcanic rock powder for application in agriculture as soil a remineralizer. *Sci Total*  
590 *Environ* 512–513, 371–380. <https://doi.org/10.1016/j.scitotenv.2014.12.070>  
591 Ritter, W.F., 1988. Reducing Impacts of Nonpoint Source Pollution from Agriculture - a Review. *J Environ Sci*  
592 *Heal A J Environ Sci Heal A* 23, 645–667.  
593 Sarabi, S., Sepaskhah, A., 2012. Effect of zeolite and saline water application on saturated hydraulic  
594 conductivity and infiltration in different soil textures. *Archives of Agronomy and Soil Science* 59, 1–  
595 12. <https://doi.org/10.1080/03650340.2012.675626>  
596 Schmidt, H.-P., 2015. European Biochar Certificate (EBC) - guidelines version 6.1.  
597 <https://doi.org/10.13140/RG.2.1.4658.7043>  
598 Sethi, R., Di Molfetta, A., 2019. GROUNDWATER ENGINEERING A Technical Approach to Hydrogeology,  
599 Contaminant Transport and Groundwater Remediation. [https://doi.org/10.1007/978-3-030-20516-](https://doi.org/10.1007/978-3-030-20516-4)  
600 4  
601 Shan, D., Deng, S., Zhao, T., Wang, B., Wang, Y., Huang, J., Yu, G., Winglee, J., Wiesner, M.R., 2016.  
602 Preparation of ultrafine magnetic biochar and activated carbon for pharmaceutical adsorption and  
603 subsequent degradation by ball milling. *Journal of Hazardous Materials* 305, 156–163.  
604 <https://doi.org/10.1016/j.jhazmat.2015.11.047>  
605 Silveira, M.L., Alleoni, L.R.F., O'Connor, G.A., Chang, A.C., 2006. Heavy metal sequential extraction  
606 methods—A modification for tropical soils. *Chemosphere* 64, 1929–1938.  
607 <https://doi.org/10.1016/j.chemosphere.2006.01.018>  
608 Simunek, J., Jacques, D., Langergraber, G., Bradford, S.A., Sejna, M., van Genuchten, M.T., 2013. Numerical  
609 Modeling of Contaminant Transport Using HYDRUS and its Specialized Modules. *J Indian I Sci* 93,  
610 265–284.  
611 Simunek, J., van Genuchten, M.T., Sejna, M., 2012. Hydrus: Model Use, Calibration, and Validation. *T Asabe*  
612 55, 1261–1274.  
613 Sud, D., Mahajan, G., Kaur, M.P., 2008. Agricultural waste material as potential adsorbent for sequestering  
614 heavy metal ions from aqueous solutions – A review. *Bioresource Technology* 99, 6017–6027.  
615 <https://doi.org/10.1016/j.biortech.2007.11.064>  
616 Tan, X., Liu, Y., Zeng, G., Wang, X., Hu, X., Gu, Y., Yang, Z., 2015. Application of biochar for the removal of  
617 pollutants from aqueous solutions. *Chemosphere* 125, 70–85.  
618 <https://doi.org/10.1016/j.chemosphere.2014.12.058>  
619 Tong, Y., McNamara, P.J., Mayer, B.K., 2019. Adsorption of organic micropollutants onto biochar: a review  
620 of relevant kinetics, mechanisms and equilibrium. *Environ. Sci.: Water Res. Technol.* 5, 821–838.  
621 <https://doi.org/10.1039/C8EW00938D>  
622 Tran, H., You, S.-J., Chao, H.-P., 2015. Effect of pyrolysis temperatures and times on the adsorption of  
623 cadmium onto orange peel derived biochar. *Waste Management & Research* 34.  
624 <https://doi.org/10.1177/0734242X15615698>  
625 Vadivelan, V., Kumar, K.V., 2005. Equilibrium, kinetics, mechanism, and process design for the sorption of  
626 methylene blue onto rice husk. *Journal of Colloid and Interface Science* 286, 90–100.  
627 <https://doi.org/10.1016/j.jcis.2005.01.007>  
628 Verheijen, F.G.A., Zhuravel, A., Silva, F.C., Amaro, A., Ben-Hur, M., Keizer, J.J., 2019. The influence of biochar  
629 particle size and concentration on bulk density and maximum water holding capacity of sandy vs  
630 sandy loam soil in a column experiment. *Geoderma* 347, 194–202.  
631 <https://doi.org/10.1016/j.geoderma.2019.03.044>  
632 Wang, J., Chen, T., Li, S., Yue, Z.-B., Jin, J., He, G., Zhang, H., 2012. Biosorption of Copper (II) from Aqueous  
633 Solutions with Rape Straw. *Geomicrobiology Journal* 29, 250–254.  
634 <https://doi.org/10.1080/01490451.2011.598603>

- 635 Wang, S.Z., Wang, J.L., 2022. Magnetic 2D/2D oxygen doped g-C<sub>3</sub>N<sub>4</sub>/biochar composite to activate  
636 peroxymonosulfate for degradation of emerging organic pollutants. *J Hazard Mater* 423.  
637 <https://doi.org/10.1016/j.jhazmat.2021.127207>
- 638 Waqas, M., Asam, Z.-Z., Rehan, M., Anwar, M., Khattak, R., Ismail, I., Tabatabaei, M., Nizami, Dr.A.-S., 2021.  
639 Development of biomass-derived biochar for agronomic and environmental remediation  
640 applications. *Biomass Conversion and Biorefinery* 11, 1–23. <https://doi.org/10.1007/s13399-020-00936-2>
- 642 Yan, Y., Akbar Nakhli, S.A., Jin, J., Mills, G., Willson, C.S., Legates, D.R., Manahiloh, K.N., Imhoff, P.T., 2021.  
643 Predicting the impact of biochar on the saturated hydraulic conductivity of natural and engineered  
644 media. *Journal of Environmental Management* 295, 113143.  
645 <https://doi.org/10.1016/j.jenvman.2021.113143>
- 646 Zand, A.D., Abyaneh, M.R., 2020. Adsorption of Lead, manganese, and copper onto biochar in landfill  
647 leachate: implication of non-linear regression analysis. *Sustainable Environment Research* 30, 18.  
648 <https://doi.org/10.1186/s42834-020-00061-9>
- 649 Zhao, S., Ta, N., Wang, X., 2020. Absorption of Cu(II) and Zn(II) from Aqueous Solutions onto Biochars  
650 Derived from Apple Tree Branches. *Energies* 13. <https://doi.org/10.3390/en13133498>
- 651 Zou, W., Han, R., Chen, Z., Jinghua, Z., Shi, J., 2006. Kinetic study of adsorption of Cu(II) and Pb(II) from  
652 aqueous solutions using manganese oxide coated zeolite in batch mode. *Colloids and Surfaces A:  
653 Physicochemical and Engineering Aspects* 279, 238–246.  
654 <https://doi.org/10.1016/j.colsurfa.2006.01.008>
- 655

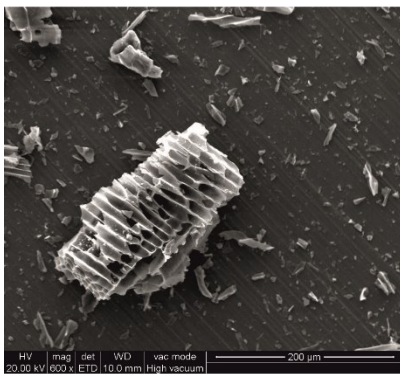
#### 656 **Acknowledgements**

657 The authors thank prof. Rajandrea Sethi for guidance and support in the study development.

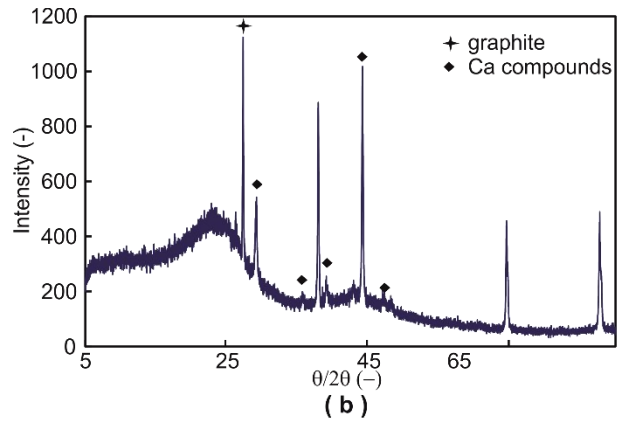
658 The part of the study concerning corncob has received funding in the framework of the project NODES from  
659 the MUR - M4C2 1.5 of PNRR funded by the European Union - NextGenerationEU (Grant agreement no.  
660 ECS00000036).

661

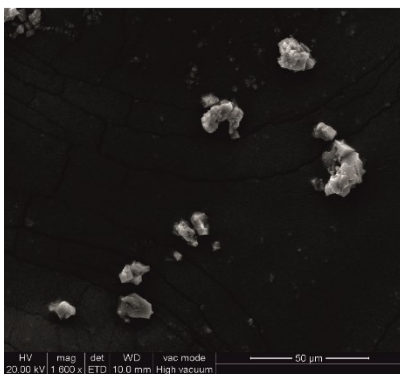
662



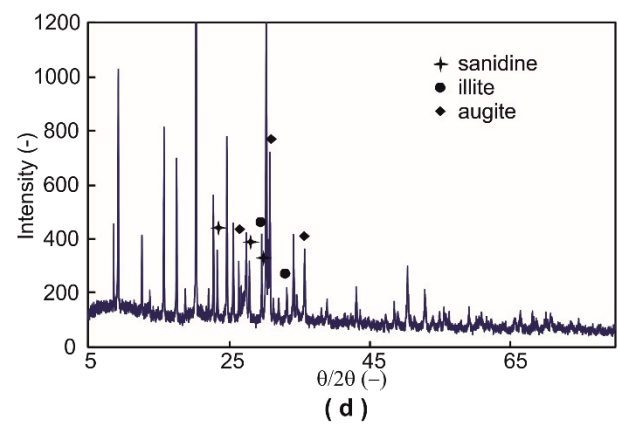
(a)



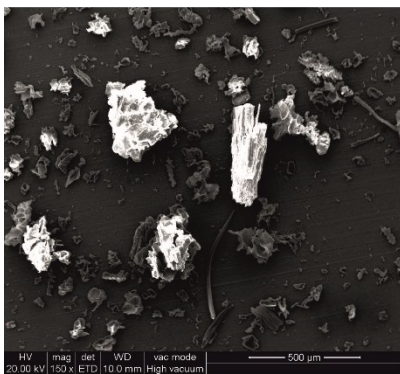
(b)



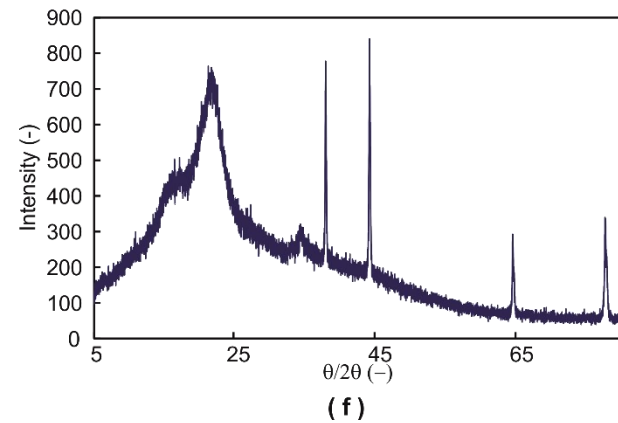
(c)



(d)



(e)

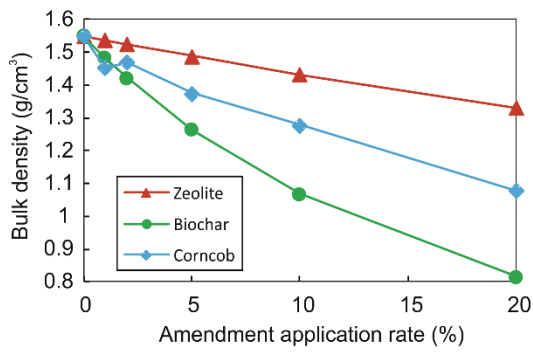


(f)

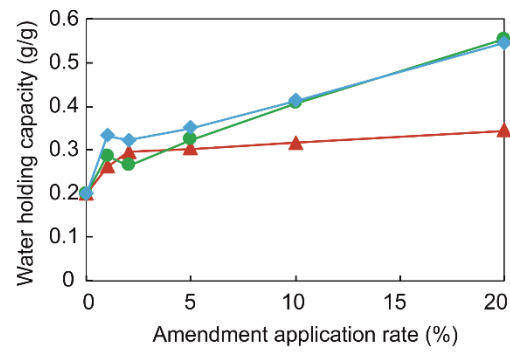
664

665 Figure 1 SEM images (a, c, e) and XRD spectra (b, d, f) for biochar (a, b), zeolite (c, d) and corncob (e, f) samples.

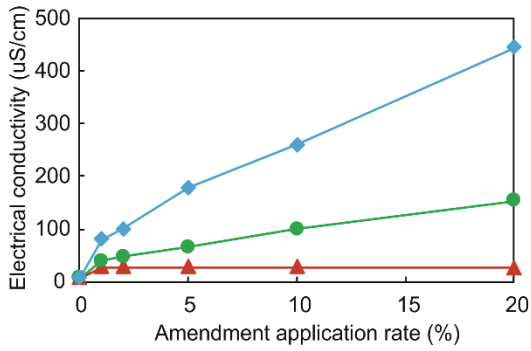
666



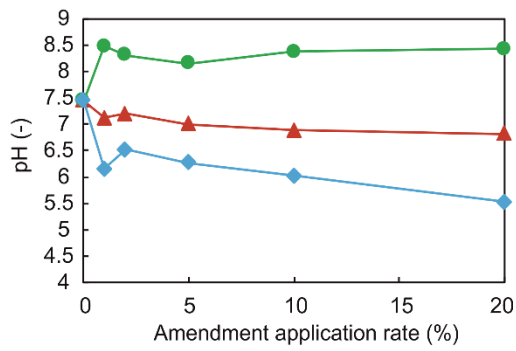
(a)



(b)



(c)

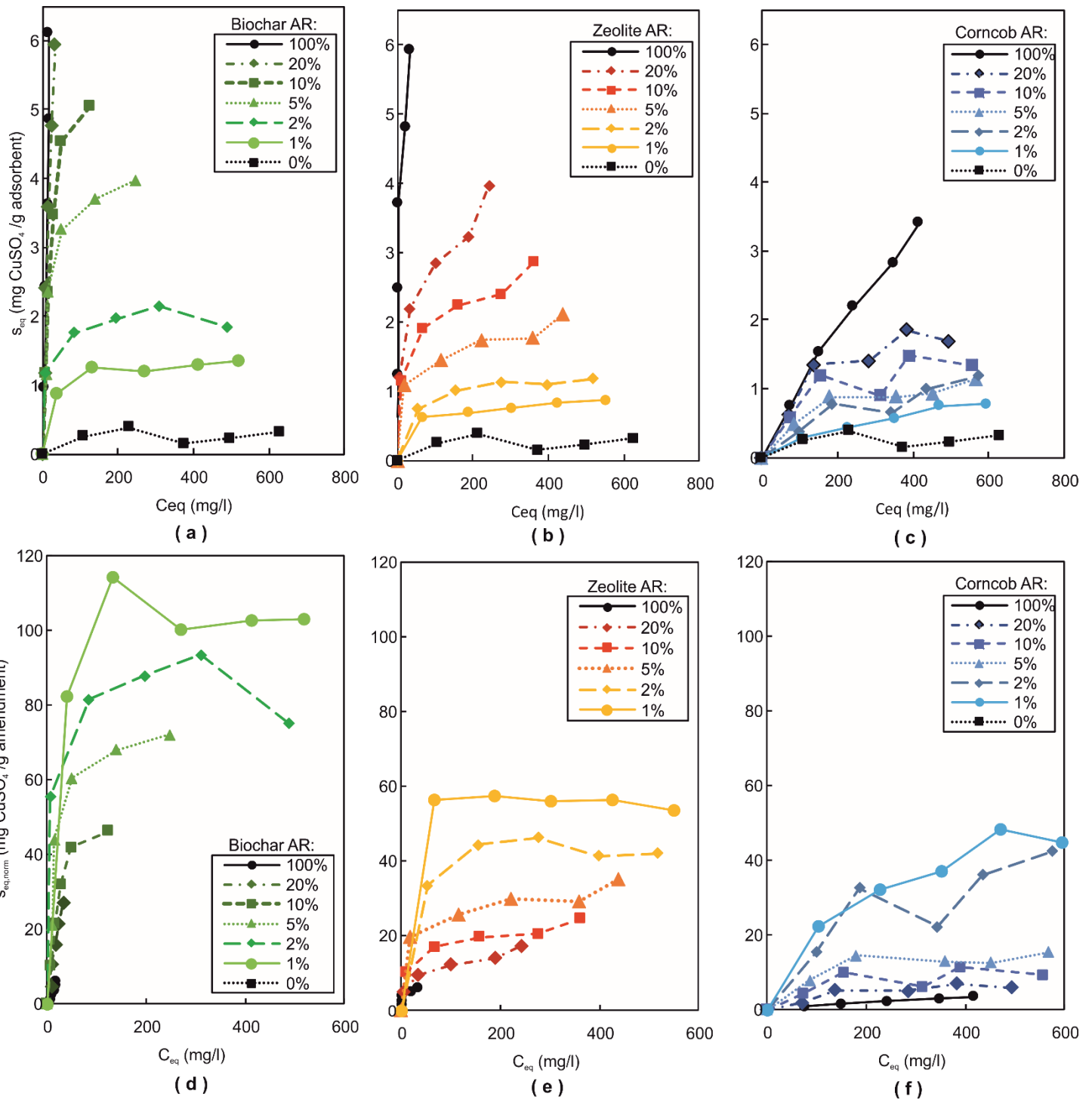


(d)

667

668 *Figure 2 Bulk density (a), water holding capacity (b), electrical conductivity (c) and pH (d) for amendment-*  
 669 *sand mixtures at different application rates*

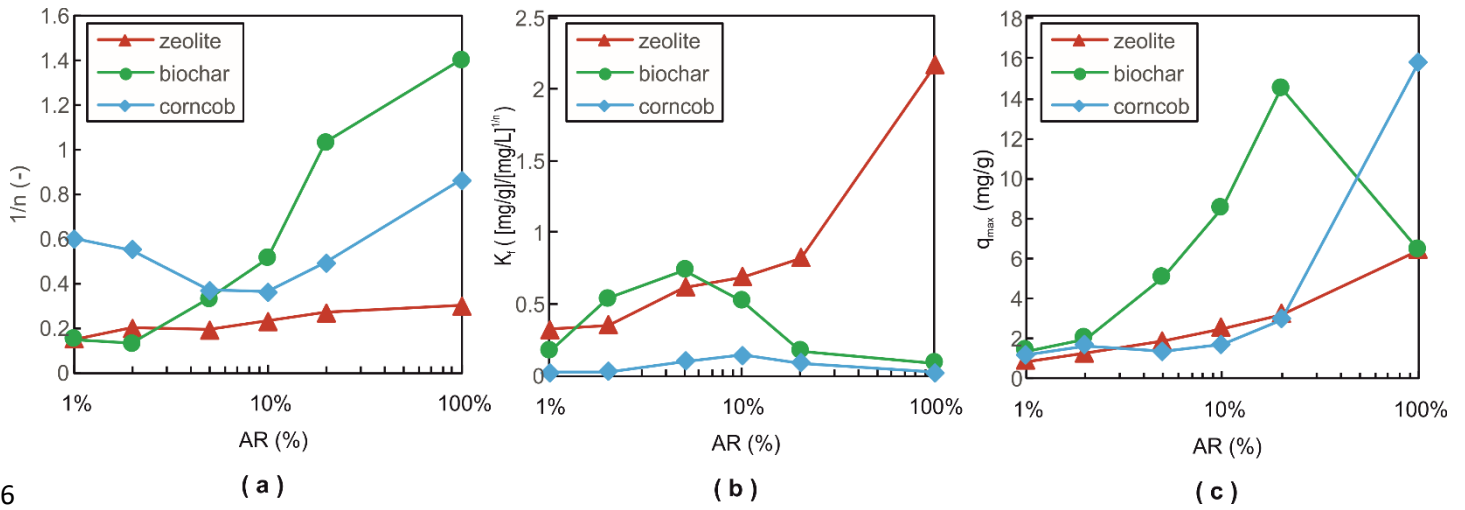
670



671

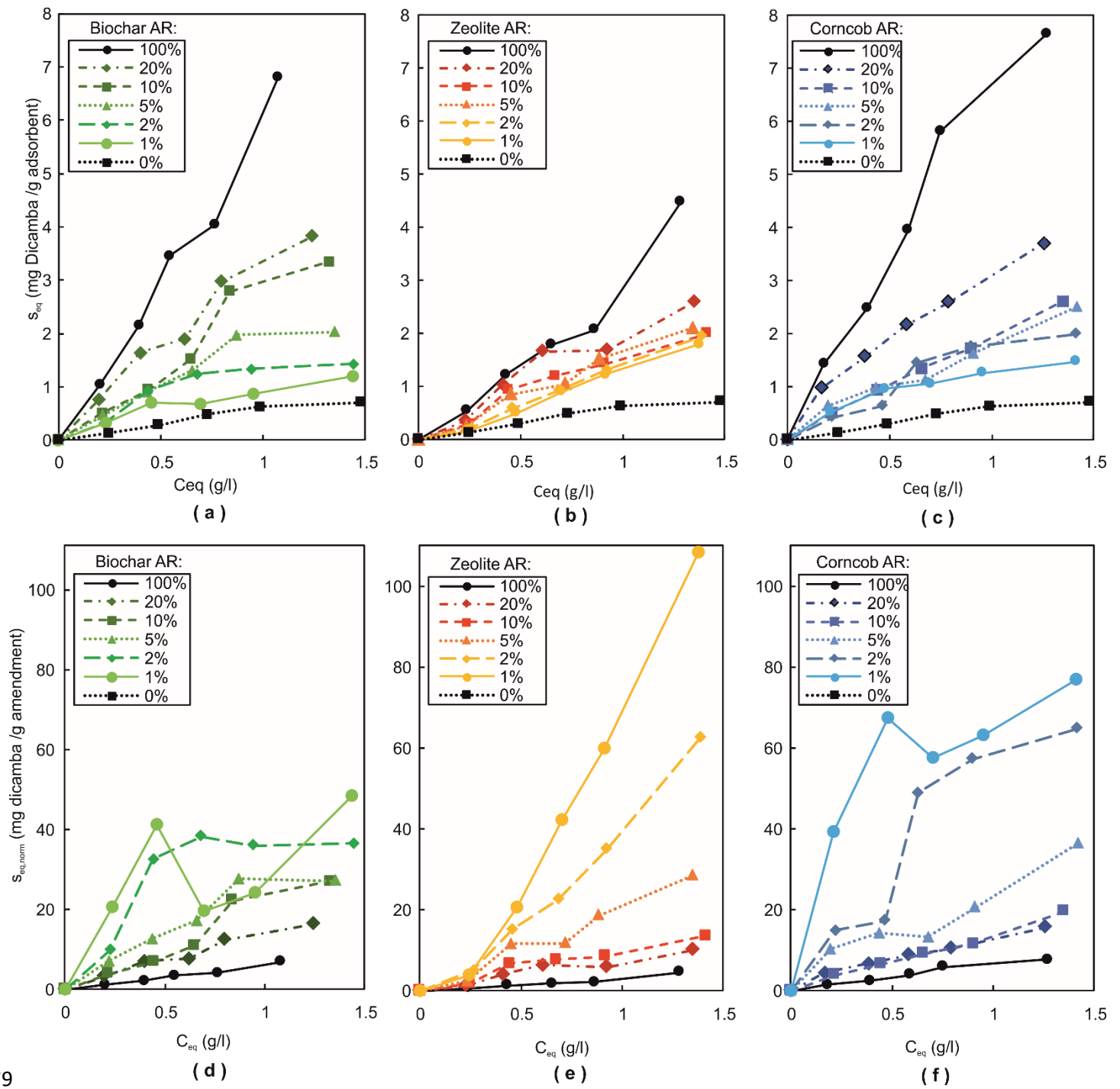
672 *Figure 3 Copper sulphate adsorption isotherms reported as adsorbed  $CuSO_4$  per total mass of adsorbent (sand*  
 673 *+ amendment) (a-c) and per total mass of amendment (d-f) vs equilibrium concentration in liquid phase, at*  
 674 *different application rates (AR), for biochar (a,d), zeolite (b,e) and corncob (c,f)*

675



676

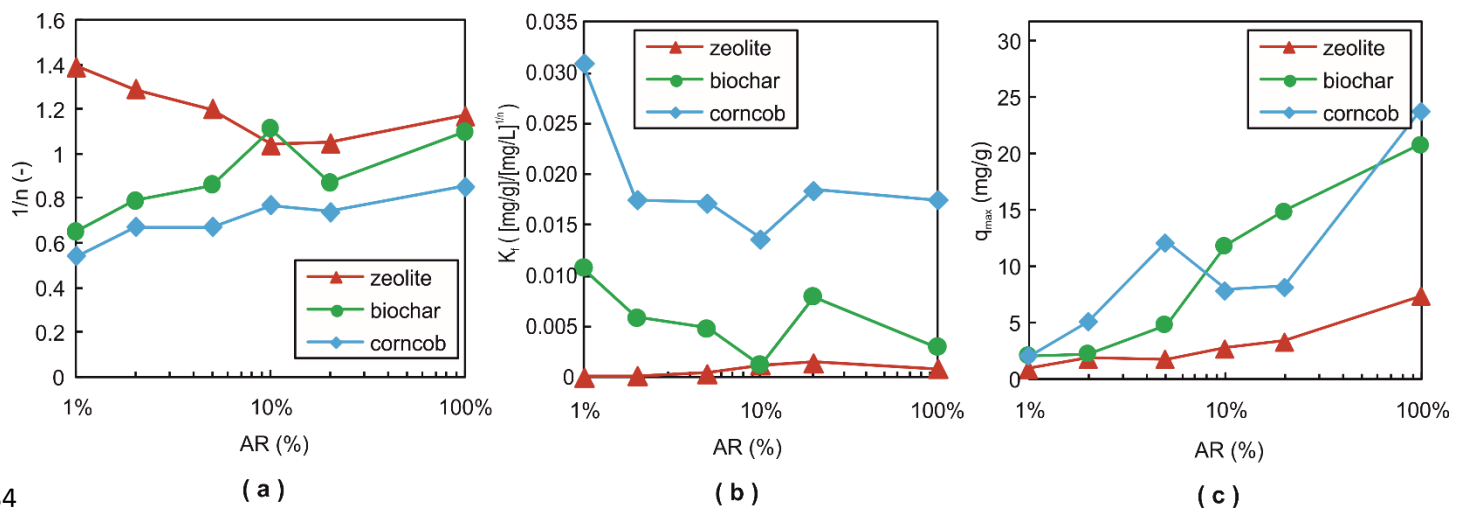
677 *Figure 4 Freundlich (a,b) and Langmuir (c) parameters for  $\text{CuSO}_4$  adsorption isotherms as a function of the*  
 678 *amendment application rate*



679

680 *Figure 5 Dicamba adsorption isotherms reported as adsorbed dicamba per total mass of adsorbent (sand +*  
 681 *amendment) (a-c) and per total mass of amendment (d-f) vs equilibrium concentration in liquid phase, at*  
 682 *different application rates (AR), for biochar (a,d), zeolite (b,e) and corncob (c,f)*

683



684

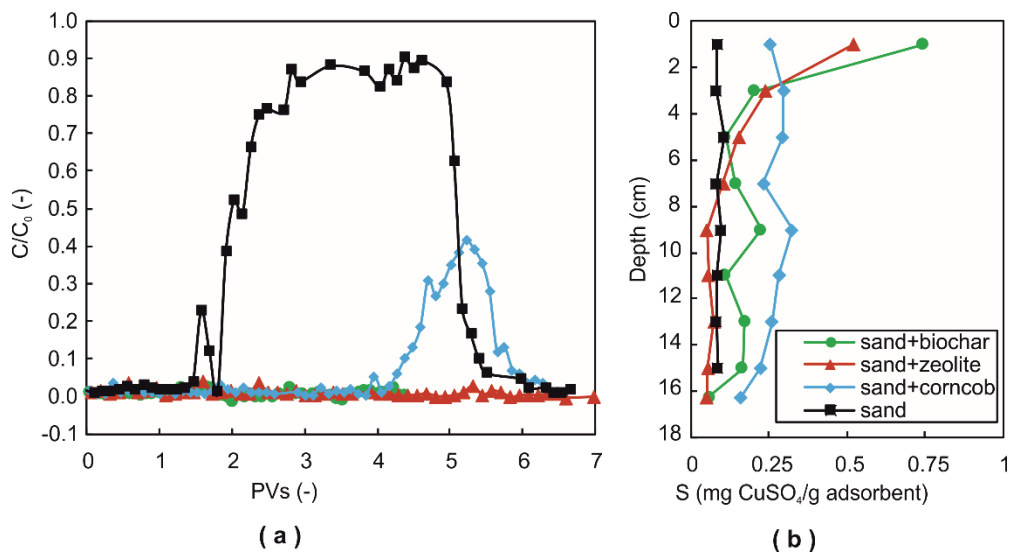
(a)

(b)

(c)

685 Figure 6 Freundlich (a,b) and Langmuir (c) parameters for dicamba adsorption isotherms as a function of the  
 686 amendment application rate

687



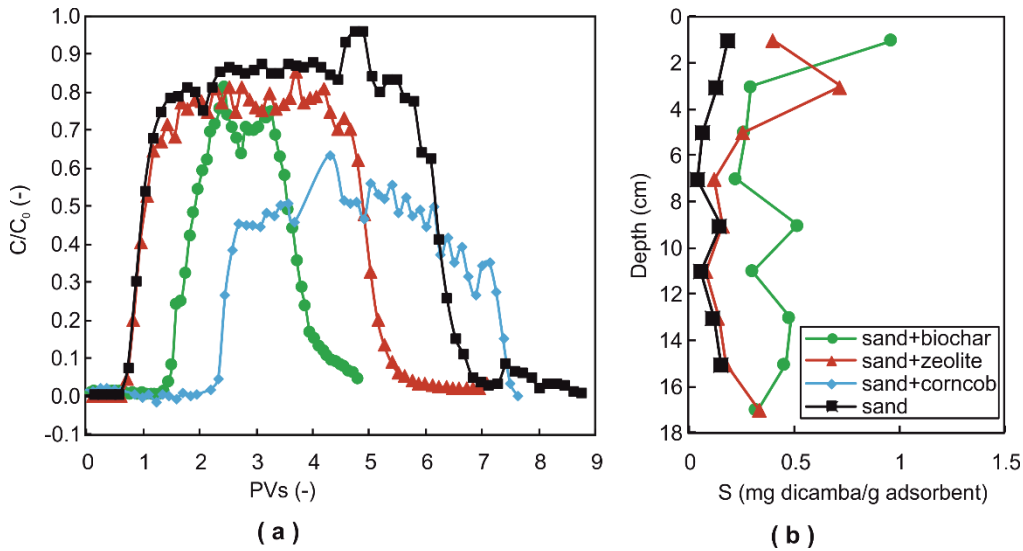
688

(a)

(b)

689 Figure 7 Normalized  $CuSO_4$  breakthrough curve ( $C/C_0$  as a function of the number of injected pore volumes  
 690 PVs) (a) and final vertical profile of adsorbed  $CuSO_4$  (mass concentration  $S$  versus depth) (b) for sand and sand-  
 691 amendment column leaching tests. The injection starts at PV = 0 (column pre-conditioning and tracer tests  
 692 are not reported)

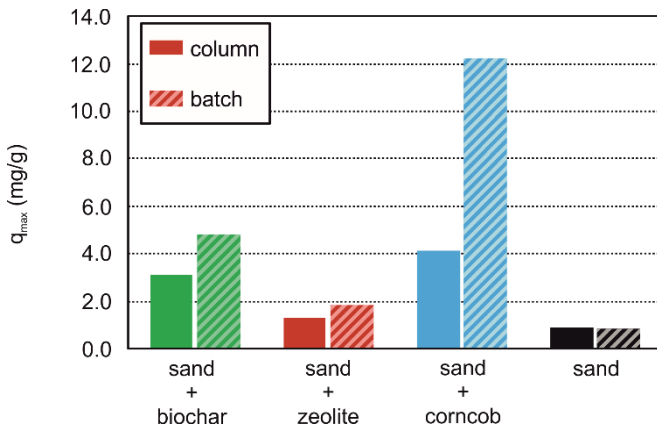
693



694

695 *Figure 8 Normalized dicamba breakthrough curve ( $C/C_0$  as a function of the number of injected pore volumes*  
 696 *PVs) (a) and final vertical profile of adsorbed dicamba(mass concentration  $S$  versus depth) (b) for sand and*  
 697 *sand-amendment column leaching tests. The injection starts at PV = 0 (column pre-conditioning and tracer*  
 698 *tests are not reported)*

699



700

701 *Figure 9 Comparison of maximum adsorption capacity  $q_{max}$  obtained via fitting of breakthrough curves of*  
 702 *column transport tests (solid bars) and of adsorption isotherms of batch tests (dashed bars) of dicamba*  
 703 *solutions in contact with sand-amendment mixtures (application rate equal to 5%) and pure sand.*

704

705 **TABLE CAPTION**706 *Table 1 Column leaching tests: geometrical characteristics, hydrodynamic parameters and mass balance*  
707 *results*

708

	<b>Sand</b>	<b>Zeolite-sand</b>	<b>Biochar-sand</b>	<b>Corncob-sand</b>
<b>CuSO<sub>4</sub></b>				
<b>Column length (cm)</b>	15	16.5	18	18
<b>Bulk density (g/cm<sup>3</sup>)</b>	1.54	1.40	1.28	1.28
<b>Porosity (-)</b>	0.41	0.42	0.485	0.44
<b>Pore volume PV (min)</b>	132	117	193	142
<b>Unsaturated water content (-)</b>	0.22	0.216	0.32	0.23
<b>Saturated hydraulic conductivity K<sub>sat</sub> (m/s)</b>	7.92·10 <sup>-5</sup>	5.72·10 <sup>-5</sup>	2.59·10 <sup>-5</sup>	5.88·10 <sup>-5</sup>
<b>Hydrodynamic dispersivity α (m)</b>	4.16·10 <sup>-3</sup>	5.38·10 <sup>-3</sup>	5.99·10 <sup>-3</sup>	2.85·10 <sup>-3</sup>
<b>Leached CuSO<sub>4</sub> (%)</b>	56	1.2	1.1	10.2
<b>Recovered CuSO<sub>4</sub> (leached + extracted) (%)</b>	101.4	37.7	53.4	75.6
<b>Dicamba</b>				
<b>Column length (cm)</b>	15.4	17	18.2	18.5
<b>Bulk density (g/cm<sup>3</sup>)</b>	1.50	1.36	1.27	1.25
<b>Porosity (-)</b>	0.40	0.41	0.48	0.44
<b>Pore volume PV (min)</b>	101	125	197	122
<b>Unsaturated water content (m<sup>3</sup>/m<sup>3</sup>)</b>	0.19	0.21	0.31	0.2
<b>Saturated hydraulic conductivity K<sub>sat</sub> (m/s)</b>	1.01·10 <sup>-4</sup>	6.32·10 <sup>-5</sup>	2.70·10 <sup>-5</sup>	9·10 <sup>-5</sup>
<b>Hydrodynamic dispersivity α (m)</b>	4.67·10 <sup>-3</sup>	4.34·10 <sup>-3</sup>	4.32·10 <sup>-3</sup>	7.58·10 <sup>-3</sup>
<b>Leached dicamba (%)</b>	87	70	45.4	44
<b>Recovered dicamba (leached + extracted) (%)</b>	99	98.1	45.4*	88.9

709 \* Dicamba vertical profile was not determined